Neurotoxicology 94 (2023) 46–58

Contents lists available at ScienceDirect

Neurotoxicology

journal homepage: www.elsevier.com/locate/neuro

Acute radiofrequency electromagnetic radiation exposure impairs neurogenesis and causes neuronal DNA damage in the young rat brain

Kumari Vandana Singh [a], Chandra Prakash [b], Jay Prakash Nirala [a], Ranjan Kumar Nanda [c,*], Paulraj Rajamani [a,**]

[a] School of Environmental Sciences, Jawaharlal Nehru University, New Delhi 110067, India
[b] School of Life Sciences, Jawaharlal Nehru University, New Delhi 110067, India
[c] Translational Health Group, International Center for Genetic Engineering and Biotechnology, New Delhi 110067, India

ARTICLE INFO

Edited by Dr. Lucio Costa

Keywords:
Cerebral cortex
Hippocampus
Neurogenesis
Oxidative stress
RF-EMR

ABSTRACT

A mobile phone is now a commonly used device for digital media and communication among all age groups. Young adolescents use it for longer durations, which exposes them to radiofrequency electromagnetic radiation (RF-EMR). This exposure can lead to neuropsychiatric changes. The underlying cellular mechanism behind these changes requires detailed investigation. In the present study, we investigated the effect of RF-EMR emitted from mobile phones on young adolescent rat brains. Wistar rats (5 weeks, male) were exposed to RF-EMR signal (2115 MHz) at a head average specific absorption rate (SAR) of 1.51 W/kg continuously for 8 h. Higher level of lipid peroxidation, carbon-centered lipid radicals, and single-strand DNA damage was observed in the brain of rat exposed to RF-EMR. The number of BrdU-positive cells in the dentate gyrus (DG) decreased in RF-EMR-exposed rats, indicating reduced neurogenesis. RF-EMR exposure also induced degenerative changes and neuronal loss in DG neurons but had no effect on the CA3 and CA1 neurons of the hippocampus and cerebral cortex. The activity of Pro-caspase3 did not increase upon exposure in any of the brain regions, pointing out that degeneration observed in the DG region is not dependent on caspase activation. Results indicate that short-term acute exposure to RF-EMR induced the generation of carbon-centered lipid radicals and nuclear DNA damage, both of which likely played a role in the impaired neurogenesis and neuronal degeneration seen in the young brain's hippocampus region. The understanding of RF-EMR-induced alteration in the brain at the cellular level will help develop appropriate interventions for reducing its adverse impact.

1. Introduction

By 2022, worldwide ~8.65 billion mobile phone subscriptions are available with the majority (6.38 billion) using smartphones (https://www.statista.com). Adolescents (8–18 years of age) reported spending around 8 h a day on smartphones (Common Sense Media, 2019). The third-generation (3 G) smartphones operate at a frequency range of 1.8–2.5 GHz with Wideband Code Division Multiple Access (WCDMA) standard and fourth-generation (4G) phones, operate at a higher frequency range of 2–8 GHz with Long-term Evolution (LTE) standard (Kesari et al., 2014; Miller et al., 2019). Specific absorption rate (SAR) is the primary measure of exposure used to estimate the absorption of radiofrequency electromagnetic radiation (RF-EMR) by animal tissue. Many present-day mobile phones have a maximum SAR close to 1.5 W/kg for the head (https://www.bfs.de/). Evidence from epidemiological studies suggests that the use of smartphones by people, especially in the adolescent age group, is associated with cognitive decline and behavioral and emotional disorders (De-Sola Gutierrez et al., 2016; Foerster et al., 2018; Stein and Udasin, 2020; Sudan et al., 2016). Generation of oxidative stress, DNA damage, inhibition of DNA

Abbreviations: BrdU, 5-Bromo-2′-deoxyuridine; CA, Cornu ammonis; CV, Cresyl violet; C•, Carbon centered radical; DG, Dentate gyrus; LPO, Lipid Peroxide; NPCs, Neural progenitor cells; PUFA, Polyunsaturated fatty acid; RF-EMR, Radiofrequency electromagnetic radiation; ROS, Reactive oxygen species; SAR, Specific absorption rate.

* Correspondence to: Translational Health Group, International Centre for Genetic Engineering and Biotechnology (ICGEB), New Delhi Component, Aruna Asaf Ali Marg, 110067, India.
** Corresponding author.
E-mail addresses: ranjan@icgeb.res.in (R.K. Nanda), paulrajr@mail.jnu.ac.in (P. Rajamani).

https://doi.org/10.1016/j.neuro.2022.11.001
Received 17 June 2022; Received in revised form 2 November 2022; Accepted 2 November 2022
Available online 3 November 2022
0161-813X/© 2022 Published by Elsevier B.V.

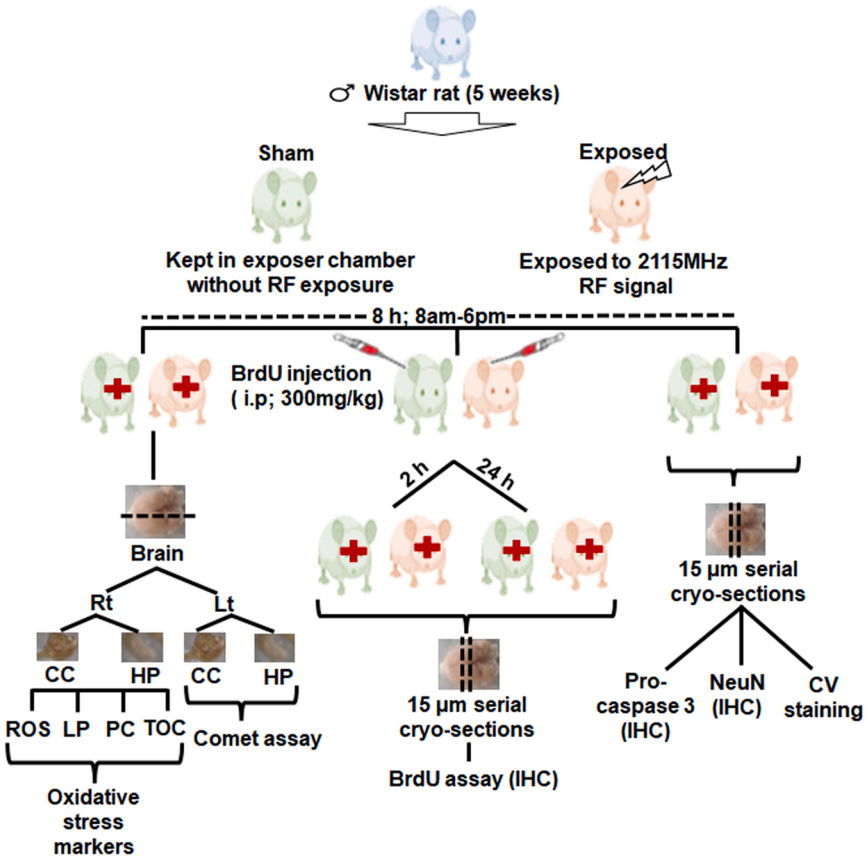


Fig. 1. Workplan adopted to study the effect of radio-frequency electromagnetic radiation (RF-EMR) exposure for 8 h on the developing brain of Wistar rats. A total of twenty-six rats were divided into two groups, 1) Sham and 2) Exposed. Out of thirteen rats from each group, four were used to study oxidative stress parameters (one hemisphere) and comet assay (another hemisphere), and three rats for cresyl violet (CV) staining. Six rats from each group were injected with BrdU intraperitoneally (300 mg/kg) at the end of exposure time and sacrificed 2 h and 24 h post-injection (n = 3) to study hippocampal neurogenesis. BrdU: 5-Bromo-2′-deoxyuridine, CC: cerebral cortex, HP: hippocampus, LP: lipid peroxidation, PC: protein carbonylation, ROS: reactive oxygen species, TOC: total antioxidant capacity.

repair, altered gene and protein expression, epigenetic changes, and altered intracellular calcium metabolism seems to be contributing to the RF-EMR exposure-induced damage in the brain (https://bioinitiative.org/; Pall, 2018, 2012; Sage and Burgio, 2018; Singh et al., 2022). However, the cellular mechanism behind these effects in the young brain requires additional investigation.

A thin skull, lower myelin content, and higher water content leads the young brain to absorb 2–3 times higher dose of RF-EMR energy than adults (Fernandez et al., 2018; Redmayne and Johansson, 2014). Many developmental changes and ongoing maturational processes in young adolescent brains make them susceptible to RF-EMR (Belpomme et al., 2018). The cerebral cortex and hippocampus absorb maximum RF-EMR energy at higher frequencies (Cardis et al., 2008; Fernandez et al., 2018). Earlier studies have suggested an adverse effect of RF-EMR on cognitive functions associated with a brain region that receives maximum exposure during mobile phone use (Foerster et al., 2018). Signs of atrophy have been reported in the grey matter cortex of adolescents who are heavily addicted to digital media devices (Yuan et al., 2011). Further, the adult hippocampal neurogenesis, which plays a vital role in memory acquisition, is very prominent during young age and highly sensitive to early life stressors (Youssef et al., 2019), including electromagnetic radiation (Leone et al., 2014). So, the impact of RF-EMR exposure on these brain regions of the young brain need focused studies.

The intensity of RF-EMR emitted from mobile phones is much below the limiting guidelines to cause a thermal effect (Hyland, 2000). However, the non-thermal effects of RF-EMR on the brain and other tissues have long been established (Belyaev et al., 2016; De Lorge, 1979; Fragopoulou et al., 2018; Kim et al., 2019; Pall, 2016; Yang et al., 2022). The non-thermal effects of RF-EMR on the biological system largely depend on carrier frequency and modulation (Panagopoulos et al., 2013). Other factors like the intensity, duration of exposure, physiological parameters, and developmental stage of animals modulate the biological effects (Belyaev, 2010). Like, certain oscillatory frequencies of non-thermal RF-EMR may interfere with the nervous system's endogenous electric field (Wainwright, 2000), which is particularly detrimental to the proliferation and differentiation of neurons in the young brain (Levin, 2003). Incidences of glioma have been reported in the actively dividing glial cells of the young brain when exposed to RF-EMR without causing any significant tissue heating (Falcioni et al., 2018).

Several reports demonstrated the damaging effect of non-thermal RF-EMR on hippocampal or cortical neurons of young rats leading to learning and memory impairment (Bas et al., 2009; Deshmukh et al., 2015; Hasan et al., 2022; Sharma et al., 2019). The pathophysiological responses of low-intensity RF-EMR are reported to produce via the downstream effect of calcium channel activation on the peroxynitrite-oxidative stress pathway (Pall, 2018). Many in vitro and in vivo studies have shown that long-term exposure to mobile phone radiation cause oxidative stress in the brain (Dasdag and Akdag, 2016, 2020) and can induce oxidative damage to cellular DNA (https://bioinitiative.org/; Belyaev, 2015; IARC, 2013). However, reports on the effect of RF-EMR exposure on hippocampal neurogenesis are limited and need additional investigation (Kim et al., 2015; Xu et al., 2017). The majority of the available reports have focused on understanding the long-term consequences of RF-EMR exposure. These studies have a limitation of missing damage partly corrected or adopted by the organism and may not be able to characterize the early loss of function. Therefore, in this study, we employed a comprehensive approach to estimating oxidative stress, DNA damage, neuronal degeneration in cortex and hippocampus regions of the brain, and the proliferation of hippocampal neural progenitor cells (NPCs) simultaneously. Male Wistar rats of age comparable to young adolescents were subjected to RF-EMR in an exposure set up mimicking short-term acute exposure (8 h continuously) from a smartphone (2115 MHz) operating at a higher SAR

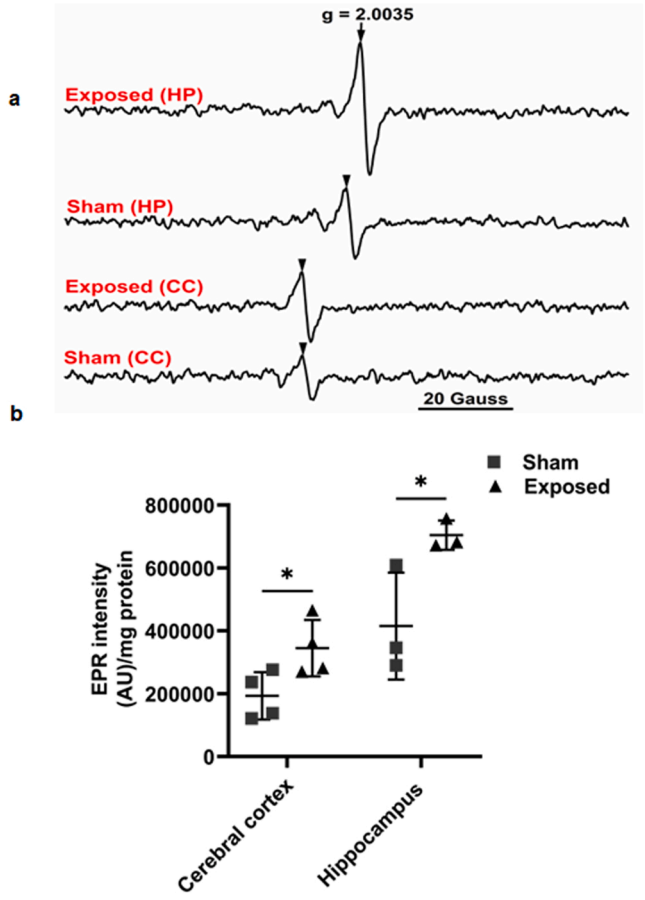


Fig. 2. Exposure to radiofrequency electromagnetic radiation (RF-EMR) for 8 h increased the level of carbon cantered free radicals in the developing rat brain. a. Representative images of electron paramagnetic resonance (EPR) spectra showing a clear peak of g = 2.0035 radical species in the cerebral cortex (CC) and hippocampus (HP) region of sham and RF-EMR-exposed rats. b. A Scatter dot plot is showing a statistical comparison of EPR signal intensity between groups (n = 4). EPR signal intensity was obtained by measuring peak to peak height of the central signal which is an estimate of radical concentration and expressed in arbitrary units (a.u.)/mg protein. Data presented as mean ± standard error of the mean (SEM). Two-tailed unpaired t-test. *P ≤ 0.05, significantly different from the sham group.

value (Head averaged SAR value of 1.51 W/kg). In this study, the specific exposure parameters and duration were chosen to simulate the worst-case scenario of short-term acute exposure from a smartphone in actual human uses.

2. Methodology

2.1. Animals and experimental plan

Animal experiments were carried out following procedures approved by the Institutional Animal Ethical Committee (IAEC) of Jawaharlal Nehru University, New Delhi, India (Application code # 23/2016). A total of 26 male Wistar rats of age 5 weeks were acquired from Central Laboratory Animal Resources, Jawaharlal Nehru University, New Delhi, and housed under 12 h light-dark cycle at 25 °C room temperature with food and water provided ad libitum. After one week of habituation, animals were randomly divided into sham and exposed groups and housed in a group of two animals per cage. A schematic presentation of the experimental plan adopted in this study is illustrated in Fig. 1.

2.2. Radiofrequency exposure

Study animals of the exposed group were subjected to RF-EMR once for 8 h continuously between 6 a.m. and 2 p.m. Exposure set up consists of a vector signal generator (VSG25A, Sigma Hound, USA) emitting 2115 MHz RF-EMR with digital modulation (16 QAM) through a horn antenna (10 cm diameter). The horn antenna was placed inside a specially designed anechoic chamber (1 m × 1 m ×1.5 m). During the exposure experiment, animals were placed in plexiglass rockets (5–7.5 cm × 20 cm × 6–8 cm) arranged in a circle inside the chamber with their truncated cones just below the center of horn antennae to allow equal exposure of all animals simultaneously (Appendix A Fig. S1). Perpendicular distance of the plexiglass rockets from the antenna was kept at 6 cm to meet the nearfield exposure condition following the equation $r \leq 2D^2/\lambda$, where r is the distance between the source of radiation and irradiated subject, D is the diameter of the antenna, and λ is the wavelength of emitted RF-EMR. Each rocket is spacious enough to allow free body movement of animals and has holes (1 cm diameter) on the upper and four sides to facilitate airflow. Receiving frequency and power at the level of rat body surface were measured using a monopole probe attached to a spectrum analyzer (N9912A, Field fox, Agilent technology, USA). The power density was measured by a power meter (NBM-520, Narda, Germany) both outside and inside the cage to adjust the fluctuation, if any, during the exposure. Attenuation due to plexiglass sheet (2 mm) comes out to be 0.11 mW/cm^2. So, the power density at the cage level (outer side) was kept at 1.11 mW/cm^2 to maintain an adequate power density of 1 mW/cm^2 inside the cage. The head averaged SAR was estimated according to the equation explained in the earlier report (Durney et al., 1979). The following equation was used, which is an expression of average SAR for the incident power density of 1 mW/cm^2 and electric field (E) field polarization for a spheroid with length and width of the animal head taken as *semimajor* axis, a, and *semiminor* axis, b, in meters.

$$SAR \quad (W/Kg) = \frac{A_1 \frac{f^2}{f_0^2}\left[1 + A_3\left(\frac{f}{f_0)u(f-f_{01}) + A_4 A_5\left(\frac{f^2}{f_0^2)u(f-f_{02})}\right)\right]}{\frac{10^3 f^2}{f_0^2} + A_2\left(\frac{f^2}{f_0^2} - 1\right)^2}$$

Where f_0 is the resonance frequency, a function of a and b, f_{01} and f_{02} are empirically derived quantities depending on values of f_0, a, and b. u ($f - f_{0l}$) and u ($f - f_{02}$) are the unit step functions. A1, A2, A3, and A4 are functions of a and b, and A5 is a function of ε, the complex permittivity of tissue.

The sham control group study animals were kept in the chamber under similar conditions, and duration as the exposed one the following day without RF-EMR exposure. Out of a total 26 animals, 13 were exposed to RF-EMR in the group of 4, 6, and 3 animals on alternate days (4 on day 1, 6 on day 3, 3 on day 5), and their respective sham controls were kept in the chamber on every alternate day (4 on day 2, 6 on day 4, 3 on day 6). Experimental variation was minimized by using a single exposure setup for all these experimental analyses. All the exposure parameters were tabulated in Appendix A Table S1.

2.3. Preparation of tissue homogenate

Animals (n = 4) from both groups were sacrificed immediately after 8 h of RF-EMR exposure using sodium pentobarbital (50 mg/kg, i.p.). Whole-brain was isolated, followed by rapid dissection of the cerebral cortex and hippocampus. One hemisphere was used to study oxidative stress parameters, and the other was used for the comet assay. Tissue samples were flash-frozen in liquid nitrogen and then stored at − 80 °C until the experimental analysis. For oxidative stress analysis, tissue was homogenized in ice-cold phosphate-buffered saline (PBS, 0.1 M pH 7.5)

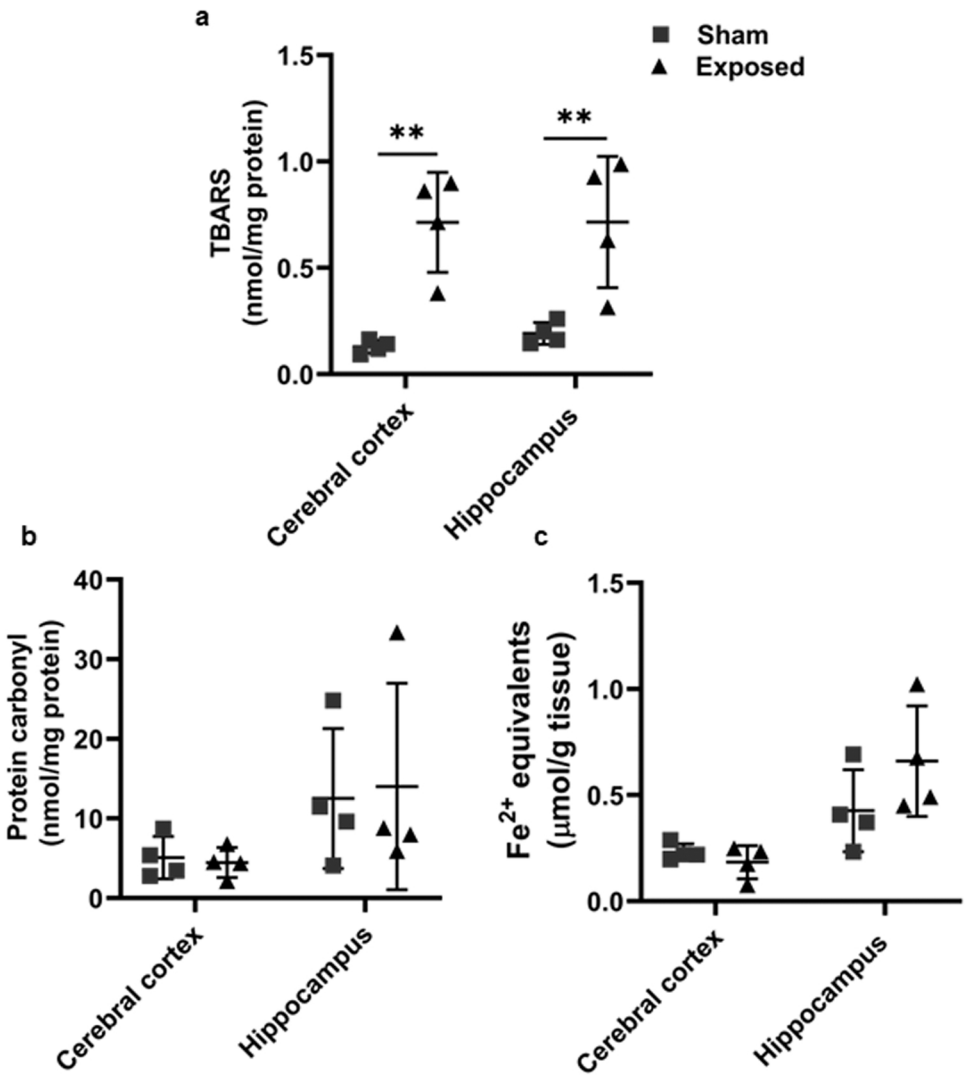


Fig. 3. Exposure to radiofrequency electromagnetic radiation (RF-EMR) for 8 h lead to increased lipid peroxidation in both the cerebral cortex (CC) and hippocampus (HP) region of the rat brain; however, the level of protein carbonyl and total antioxidant capacity (TOC) was not changed significantly in either of brain region compared to sham (n = 4). Scatter dot plots show the statistical comparison between sham and exposed groups for **a.** Lipid peroxidation in nmol TBARS/mg protein **b.** Protein carbonylation in nmol protein carbonyls/mg protein and **C.** Total antioxidant activity in µmol $FeSO_4$ equivalents/g tissue in cortex and hippocampus region of rat brain. Data presented as mean ± standard error of the mean (SEM). Two-tailed unpaired t-test. *P ≤ 0.05, **P ≤ 0.01, significantly different from the sham group.

supplemented with Diethylenetriaminepentaacetic acid (DTPA; 2 mM) as transition metal chelator and protease inhibitor cocktail (P8340, Merck, USA) using a mortar pestle at 4 °C. Homogenate was centrifuged at 1000g for 5 min at 4 °C to remove the debris, and total protein concentration was estimated using Bradford reagent (5000006, Bio-Rad, USA).

For comet assay, harvested tissues were minced using a scalpel in a 9:1 (v/v) mixture of Hanks' Balanced Salt Solution (HBSS) media (14025092, Thermo Fisher Scientific, USA) and DMSO. Next, the mixture was gently triturated with a 5 ml pipette and allowed to settle for 1 min to remove debris. The single-cell suspension thus obtained was used for the comet analysis. The entire procedure was performed within 5 min and at 4 °C to minimize DNA damage during the experimental procedure.

2.4. Electron paramagnetic resonance (EPR) spectroscopy for the detection of free radicals

Electron paramagnetic resonance (EPR) spectroscopy was performed to estimate the concentration of carbon and oxygen-centered free radicals using 5,5-Dimethyl-1-pyrroline N-oxide (DMPO) (Sigma-Aldrich, USA) a cyclic nitrone as a spin trap. Samples were prepared following the earlier published method (Rokyta et al., 2004). Briefly, tissue homogenate (54 µl) was mixed with DMPO (6 µl, 1 M) under nitrogen flow. EPR spectroscopy was performed using Bruker EMXmicroX-band (9.1–9.9 GHz) EPR spectrometer equipped with a Bruker ER 4102ST resonator/cavity maintained at 150 K using Bruker ER 4111 VT variable temperature unit. The sample mixture (30 µl) was immediately transferred to a deep-frozen X-band capillary tube (Supracil, Q-1.0 × 1.2 Wilmad-LabGlas, USA) ends were sealed. The capillary tube with the sample was immediately placed inside Bruker ER 169DIS quartz dewar in the EPR resonator so that the whole sample was vertically centered in the cavity. The spectra were recorded with the following settings: central field; 3508.8 G, sweep width; 118.8 G, resolution; 1024 points, microwave frequency; 9.8 GHz, microwave power; 13 mW, modulation frequency; 100 kHz, modulation amplitude; 1.0 G, receiver gain; 2×10^3, the time constant; 163.8 ms, sweep time; 40.9 s, conversion time; 40 ms. Spectra of each sample were acquired, and baseline corrected using WinEPR acquisition software (Version 4.3, Bruker Biospin GmbH, Germany). The reproducibility of the EPR signal was assessed in four study samples from each group. Signal intensities of radical species were determined as peak-to-peak height (arbitrary units) in the first derivative spectrum, a radical concentration measure. Data were normalized with protein concentrations and expressed as arbitrary units (a.u.)/mg protein.

2.5. Lipid peroxidation assay

Malondialdehyde (MDA) concentration was determined following the earlier reported method (Uchiyama and Mihara, 1978). Briefly,

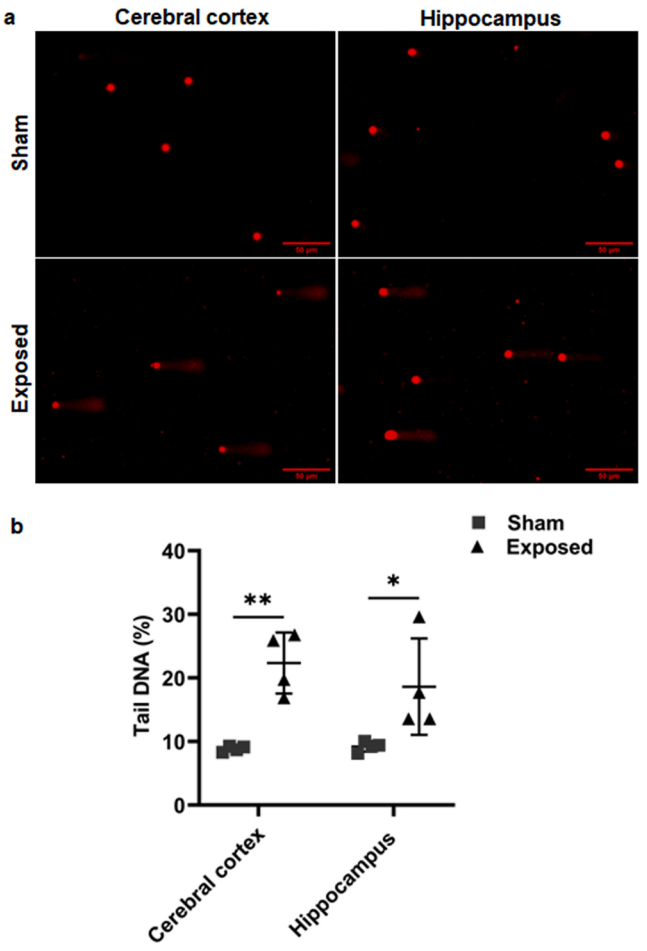


Fig. 4. Exposure to radiofrequency electromagnetic radiation (RF-EMR) for 8 h leads to single-strand DNA damage in the cerebral cortex (CC) and hippocampus (HP) region of the rat brain. a. Representative photomicrographs of comets at 40 × magnification from CC and HP region of sham and exposed animals. b. Scatter dot plot showing a statistical comparison of the percentage of total DNA (head DNA), fragmented and migrated to form a comet pattern (tail DNA) between sham and exposed groups (n = 4). The nucleus without any comet pattern was considered undamaged. For each region, tail DNA (%) was estimated in randomly selected 50 individual cells per animal using CometScore software (Version 2.01) and averaged to be used as a statistical unit to compare between groups. Data presented as mean ± standard error of the mean (SEM). Two-tailed unpaired t-test. *P ≤ 0.05, significantly different from the sham group.

tissue homogenate (125 µl) was mixed with Tris KCl Buffer (875 µl, pH 7.4) along with trichloroacetic acid (TCA; 30 %, 125 µl) and thiobarbituric acid (TBA, 52 mM, 125 µl). This solution was vortexed and incubated in the water bath at 90 °C for 60 min and cooled in tap water. TBA reactive substances (TBARS) were extracted by centrifugation at 3000*g* for 10 min. TBARS amount was determined by taking absorbance at 532 nm and was calculated as nanomole MDA equivalents per milligram of protein using the molar extinction coefficient of MDA (1.56×10^{-5} $nM^{-1}cm^{-1}$).

2.6. Protein oxidation assay

Protein oxidation in tissue homogenate was estimated following the earlier published method (Dubey et al., 1996). Briefly, the tissue homogenate (10 µl) was mixed with 2,4-Dinitrophenylhydrazine (DNPH, 40 µl, 10 nM) in HCl (2 M). The mixture was incubated for 1 h at room temperature in the dark with continuous stirring and added an equal volume of TCA (20 %) with vortexing. Thereafter, samples were kept on ice for 5 min and centrifuged at 10,000g for 10 min at 4 °C. The supernatant was discarded, and the pellet was washed once with TCA (10 %) and thrice in ethanol/ethyl acetate (1:1, v/v). Final precipitates were dissolved in guanidine hydrochloride (6 M) solution. Blank was prepared by adding HCl (2 M, 40 µl) instead of DNPH. The difference in absorbance of each sample was determined with the blank reference reading at 370 nm. The amount of protein carbonyl was calculated using a molar extinction coefficient of DNPH (2.2×10^{-5} $nM^{-1}cm^{-1}$), and the results were expressed as nanomole carbonyls per milligram of protein.

2.7. Total antioxidant capacity assay

The total antioxidant capacity of tissue homogenate was estimated by measuring the reduction of Fe^{3+} to Fe^{2+} ions (Benzie and Strain, 1996). In brief, FRAP reagent (150 µl) was mixed with tissue homogenate (5 µl) and deionized water (15 µl). After incubation for 4 min at 37 °C, the sample mixture's absorbance was taken at 593 nm. Aqueous solutions of known Fe^{2+} concentrations (0.1–1 mM) were used to generate a calibration curve. The reducing ability of the samples was calculated with reference to the reaction signal obtained from known Fe^{2+} concentrations. The values were expressed as micromole of Fe^{2+} equivalents per gram of tissue.

2.8. Comet assay

Single strand breaks in the DNA of cortical and hippocampal cells were evaluated by comet assay following the earlier described method (Lai and Singh, 1995). In brief, microscopic slides (duplicates for each sample) were coated with normal melting agarose (NMA, 0.75 %) in deionized water and thoroughly dried at room temperature. The single-cell suspension (10 µl) of tissue was mixed with low melting agarose (LMA, 0.5 %, 100 µl) in PBS at 37 °C, spread on pre-coated slides, and allowed to solidify for 10 min at 4 °C. Slides were placed in freshly prepared cold lysis buffer (2.5 mM NaCl, 100 mM EDTA, 10 mM Trizma base, 1 % Triton X, 10 % DMSO, pH 10) for 4 h at 4 °C, then immersed into cold electrophoresis buffer (300 mM NaOH, 1 mM EDTA, pH >13) for 20 min followed by electrophoresis for 25 min at 24 V. After electrophoresis, slides were drained and slowly dipped in neutralization buffer (0.4 M tris, pH 7.5) three times for 5 min each. Next, slides were fixed in chilled ethanol (100 %) for 20 min and air-dried. All the steps were performed under dim light at 4 °C. Slides were randomized and coded before scoring by an independent author. On the day of analysis, slides were rehydrated with ice-cold deionized water, stained with ethidium bromide (20 µg/ml, 20 µl) for 2 min, and covered by a coverslip. Slides were visualized at 20 x magnification under a fluorescent microscope (IX71, Olympus, Japan). Images of fifty randomly selected nuclei (25 from each slide) from each animal were analyzed by CometScore software (version 2.0). DNA damage was quantified in terms of the percentage of total DNA that is fragmented and migrated away from nuclear DNA (head DNA), forming a comet pattern called tail DNA (%). The whole nucleus without any tail is considered undamaged.

2.9. 5-Bromo-2′-deoxyuridine (BrdU) administration and cell proliferation assay

To evaluate the effect of RF-EMR exposure on the proliferation of NPCs in DG, experimental rats from each group (n = 6) were administered a single intraperitoneal injection of 5-Bromo-2′-deoxyuridine (BrdU) (Sigma, USA) at a dose of 300 mg/kg just after the end of the exposure period. Three animals from each group were sacrificed 2 h or 24 h post-injection, and the effect of RF-EMR on NPCs proliferation was monitored.

Post BrdU administration (2/24 h), rats were deeply anesthetized with an intraperitoneal injection of sodium pentobarbital (50 mg/kg) and transcardially perfused with cold PBS (0.1 M, pH 7.5) for 5 min

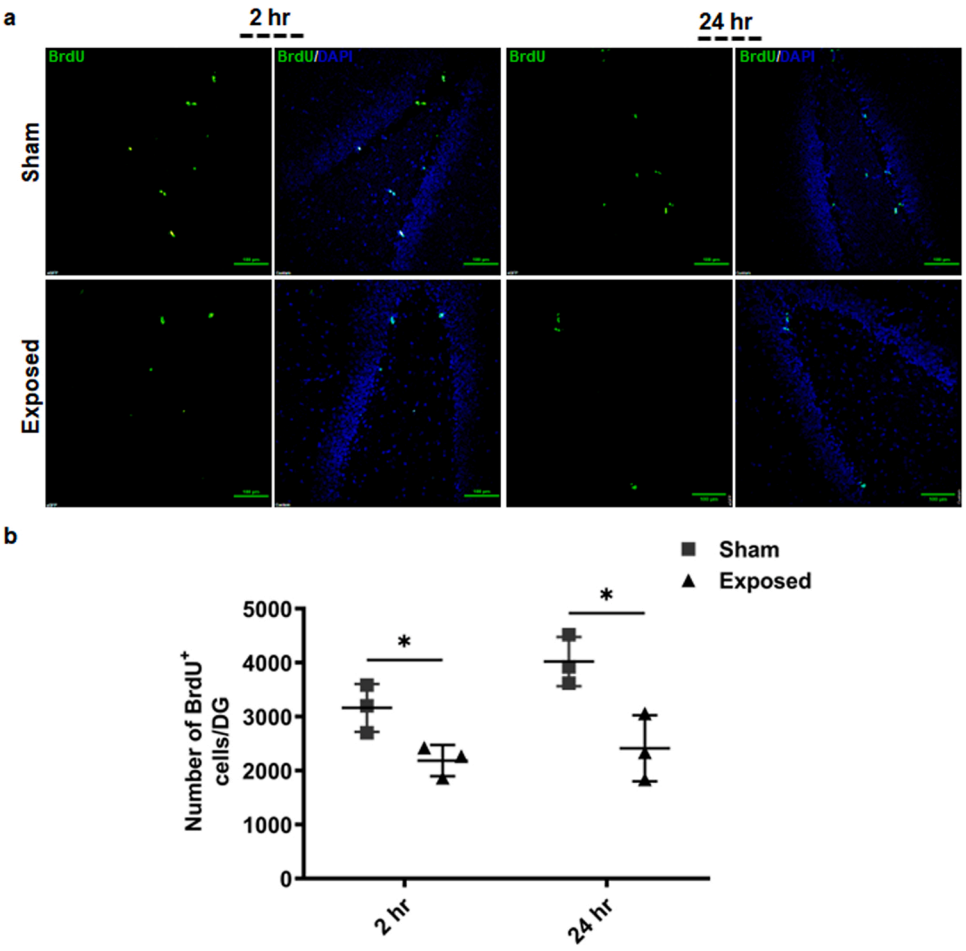


Fig. 5. Exposure to radiofrequency electromagnetic radiation (RF-EMR) for 8 h suppressed hippocampal neurogenesis in Wistar rats. a. Representative confocal images showing BrdU-positive cells (green) and counterstained nuclei (blue) in the dentate gyrus of sham and exposed rats (Scale bar=100 μm). b. The scatter dot plot is showing a statistical comparison of BrdU-positive ($BrdU^+$) cells between sham and exposed group ($n = 3$) at 2 h or 24 h post-injection time points. BrdU-positive cells in the dentate gyrus (granule cell layer and subgranular zone) were counted in every thirty-sixth section throughout the hippocampus and multiplied by 36 to obtain the total number of BrdU-positive cells per dentate gyrus per animal which is used as the statistical unit. Data presented as mean ± standard error of the mean (SEM). Two-tailed unpaired t-test. *$P \leq 0.05$, significantly different from the sham group. BrdU: 5′-bromo-2′-deoxyuridine, G: granule cell layer, H: hilus, M: molecular cell layer, S: subgranular zone.

followed by cold paraformaldehyde (2 %). The brain was harvested and fixed in paraformaldehyde (2 %) for 48 h at 4 °C, followed by immersion in sucrose solutions (10 %, 20 %, and 30 %) sequentially to cryoprotect the tissue. Next, brain tissue was embedded into Jung tissue freezing medium (Leica, Germany), and serial coronal sections were cut (15 μm thickness) through the entire hippocampus (Bregma −1.6 to −6.4) using a Cryostat (Leica CM 1860, Germany). Sections were mounted on gelatin-coated slides and were stored at − 20 °C. Every thirty-sixth section throughout the hippocampus of each rat was processed for BrdU immunofluorescence staining.

For BrdU immunofluorescence staining, slides were air-dried for 1 h at 37 °C and washed with PBS three times for 5 min each. DNA denaturation was done by placing the slides in 2 M HCl for 15 min at 37 °C. Acid was completely neutralized by three washes of PBS (pH 7.5) for 5 min each. Sections were blocked with normal goat serum (2 %, Merk Millipore, USA) for 1 h. Next, sections were incubated in a humid chamber with mouse monoclonal anti-BrdU (1:200, B35128, Invitrogen, USA) primary antibody for 24 h at 4 °C followed by three washes of PBST (0.1 %) for 5 min each. Then, sections were incubated with Alexa Fluor 488-conjugated goat anti-mouse (1:500, A11001, Invitrogen, USA) secondary antibody for 2 h in the dark at room temperature. After three washes with PBST (0.1 %) for 5 min each, slides were mounted with fluoroshield mounting medium (ab104139, Abcam, United Kingdom) containing 4′,6-diamidino-2-phenylindole (DAPI) as a counterstain and covered by a coverslip.

Slides were coded and randomized by a co-author other than the experimenter before scoring. All the BrdU-positive cells in the DG (granule cell layer and subgranular zone) were counted under a confocal microscope (FluoView™ FV1000, Olympus, Japan). BrdU-positive cells count was performed at 20× magnification. Higher magnification (100 ×) was used to distinguish single cells within a cluster. The total number of BrdU-positive cells was counted and multiplied by 36 to obtain the total number of cells per DG.

2.10. Cresyl Violet (CV) staining

Animals ($n = 3$) from each group were sacrificed immediately after the end of the exposure. Transcardial perfusion, fixation of brain tissue, and sectioning were performed as explained in the earlier section. A total of five sections from each animal at equal intervals spanning the somatosensory cortex and hippocampus were processed for CV staining. Slides with sections were air-dried and placed in alcohol chloroform solution (1:1, v/v) overnight to clear fat, followed by rehydration using alcohol (100 %, 95 %) and deionized water sequentially. Sections were stained with CV (0.1 %) staining solution for 5 min at 37 °C and differentiated using ethanol (95 %) for 5 min. Differentiated sections were dehydrated with ethanol (100 %) for 2 min and cleared in xylene for 2 min before coverslipping with DPX mounting medium. Stained sections were visualized using a light microscope (BM-Smart, Lmi Microscopes, England). Layer IV of the somatosensory cortex and different subregions of the hippocampus (DG, CA3, and CA1) were identified and delineated according to the Paxinos and Watson (2006) rat brain atlas. Images of the tissue sections from each of the subregions of interest were captured at 40× magnification. The numbers of normal neurons and degenerated neurons in each section were counted using Image J software (http://imagej.nih.gov/ij) by an experimenter blind to group codes. Neurons with large and abundant Nissl bodies were considered normal. Degenerated neurons have reduced or no Nissl body and

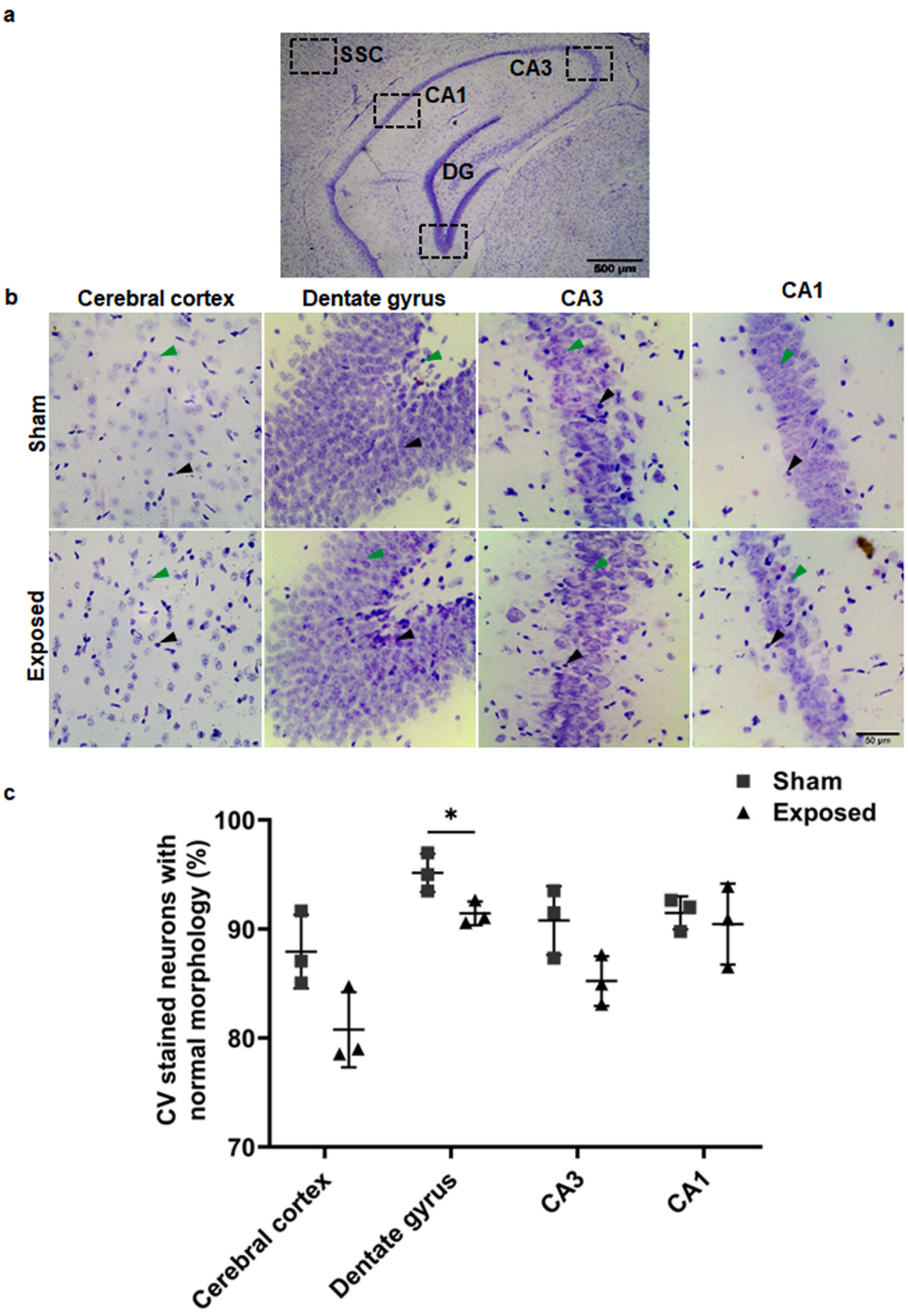


Fig. 6. Exposure to radiofrequency electromagnetic radiation (RF-EMR) for 8 h leads to degenerative changes in the dentate gyrus (DG). a. Photomicrograph of a Cresyl Violet (CV) stained coronal section (Scale bar = 500 μm) of rat brain showing somatosensory cortex and different subregions of hippocampus (CA1, CA3, and DG). Respective regions used for analysis were further delineated in boxes. b. Representative photomicrographs of CV-stained sections (Scale bar = 50 μm) of sham and exposed rats. Black and the green arrow shows pyknotic and normal neurons, respectively. c. A scatter dot plot is showing a statistical comparison of the percentage of intact neurons in the cerebral cortex and hippocampal subregions (dentate gyrus, CA1, and CA3) between sham and exposed groups (n = 3). Images from each section and each region of interest were captured at 40 x magnification and analyzed using Image J software to count the total number of normal and pyknotic neurons. The mean cell count (presented as a percentage of normal neurons) from five sections per animal was used as a statistical unit. Data presented as mean ± standard error of the mean (SEM). Two-tailed unpaired t-test. *P ≤ 0.05, significantly different from the sham group. CA: Cornu ammonis, SSC: somatosensory cortex.

showed heterogeneous morphology, including nuclear pyknosis, karyorrhectic nuclei and large vacuoles. Data were presented as a percentage of normal neurons out of total neurons, including degenerated and normal neurons.

2.11. NeuN Immunofluorescence staining

To evaluate the effect of RF-EMR on mature neurons, the expression of neuronal nuclear antigen (NeuN) in cortical and hippocampal neurons was estimated using a standard immunohistochemical procedure. Briefly, coronal sections from each animal (n = 3) were permeabilized with 10 % Triton X100 for 10 min at RT followed by blocking with 3 % normal goat serum (Merck Millipore, USA) in 0.1 % PBST for 2 h at room temperature. Subsequently, sections were incubated with NeuN Rabbit monoclonal primary antibody (1:150, DTS3I, CST, USA) overnight at 4 °C. After three washes of PBST (0.1 %) for 5 min each, sections were incubated with Alexa Fluor 594-conjugated anti-rabbit IgG (1:500, 8889, CST, USA) secondary antibody for 2 h in the dark at room temperature. After washing 3 times with PBST (0.1 %) for 5 min each, sections were mounted with fluoroshield mounting medium (ab104139, Abcam, United Kingdom) containing 4′,6-diamidino-2-phenylindole (DAPI) as a counterstain and coverslipped. Sections were visualized under a fluorescent microscope (Nikon Eclipse 90i, Tokyo, Japan) at 20× magnification. Three images were sampled per animal and NeuN intensity was calculated using Image J software after background correction by an experimenter blind to the study group. The level of

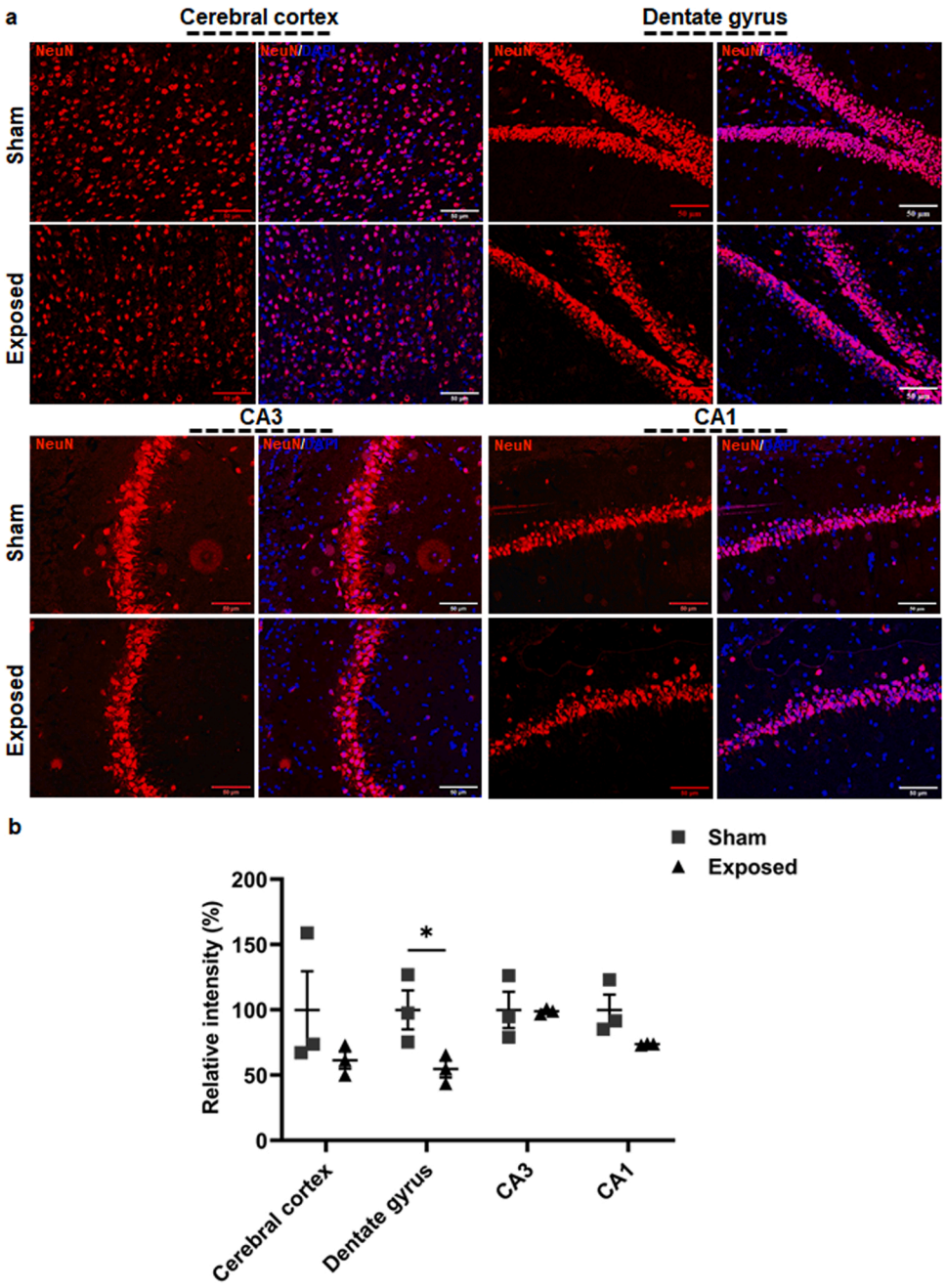


Fig. 7. Exposure to radiofrequency electromagnetic radiation (RF-EMR) for 8 h causes neuronal loss in the dentate gyrus (DG). a. Representative photomicrographs of NeuN-stained sections (Scale bar = 50 μm) of sham and exposed rats. b. The scatter dot plot is showing a statistical comparison of the relative (%) NeuN intensity in the cerebral cortex and hippocampal subregions (dentate gyrus, CA1, and CA3) with respect to sham (n = 3). Images from each section and each region of interest were captured at 20X magnification and analyzed using Image J software to calculate the fluorescent Intensity after background subtraction. The mean intensity from three images per animal (presented as a percentage of sham) was used as a statistical unit. Data presented as mean ± standard error of the mean (SEM). Two-tailed unpaired t-test. *P ≤ 0.05, significantly different from the sham group. CA: Cornu ammonis,.

NeuN expression was presented as mean percentage intensity with respect to control.

2.12. Pro-caspase 3 Immunofluorescence staining

The expression of Pro-caspase 3 protein in cortical and hippocampal sections from each animal (n = 3) was estimated using immunohistochemical analysis as described in Section 2.11. We used Active/Pro-Caspase 3 Monoclonal antibody (1:200, 31A1067, Invitrogen, USA) as the primary antibody and Alexa Fluor 488-conjugated goat anti-mouse IgG (1:500, A11001, Invitrogen, USA) as the secondary antibody. Three images were sampled per animal and Image J software was used to subtract the background and calculate the Pro-caspase 3 signal intensity. Data was presented as mean percentage intensity with respect to control.

2.13. Statistical analysis

A two-tailed unpaired Student's t-test was used to compare the groups, and a p-value ≤ 0.05 was considered significant. All results were analyzed using GraphPad Prism software (version 7.01, USA) and expressed as mean ± standard error of the mean (SEM).

3. Results

3.1. Exposure to RF-EMR causes oxidative stress in rat cortex and hippocampus

EPR spectra of cortex and hippocampus tissue homogenate showed the dominance of a broad central signal, centered on g = 2.0035 (Fig. 2a). This value of the g-factor denotes carbon-centered radicals with adjacent oxygen in the sample (Barclay and Vinqvist, 1994). A

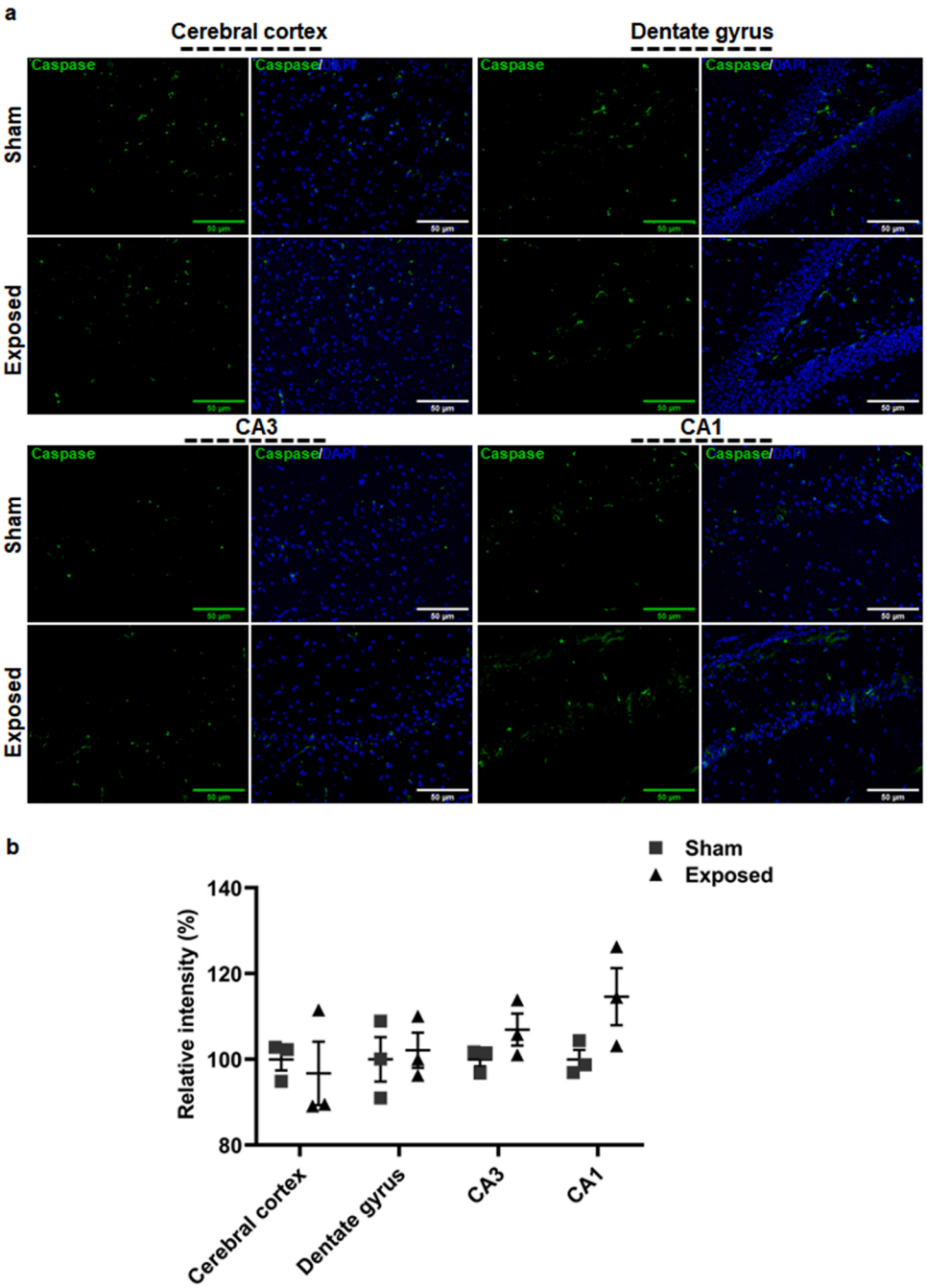


Fig. 8. Exposure to radiofrequency electromagnetic radiation (RF-EMR) for 8 h does not cause Pro-caspase3 activation in any of the brain regions studied. a. Representative photomicrographs of Pro-caspase3 immunostained sections (Scale bar = 50 μm) of sham and exposed rats. b. The scatter dot plot is showing a statistical comparison of the relative (%) Pro-caspase3 intensity in the cerebral cortex and hippocampal subregions (dentate gyrus, CA1, and CA3) with respect to sham (n = 3). Images from each section and each region of interest were captured at 20X magnification and analyzed using Image J software to calculate the fluorescent Intensity after background subtraction. The mean intensity from three images per animal (presented as a percentage of sham) was used as a statistical unit. Data presented as mean ± standard error of the mean (SEM). Two-tailed unpaired t-test. *P ≤ 0.05, significantly different from the sham group. CA: Cornu ammonis,.

comparison of the radical signal's peak-to-peak amplitude demonstrated a significant increase in g = 2.0035 radical concentration in the cortex and hippocampus of RF-EMR exposed rats compared to sham (Fig. 2b).

Lipid peroxides are the measure of the oxidative hippocampus of the rat brain exposed to RF-EMR compared to sham. Lipid peroxides level increased significantly in both cortex and the hippocampus region following RF-EMR exposure (Fig. 3a). The level of protein carbonyls represents the quantity of oxidized protein. No significant alteration in protein carbonyl concentration was observed in either the cortex or hippocampus region of rat brain exposed to RF-EMR than shams (Fig. 3b). Similarly, the change in the cortex and hippocampus region's antioxidant capacity upon RF-EMR exposure was non-significant (Fig. 3c).

3.2. Exposure to RF-EMR damages DNA in the cortex and hippocampus of rat

Cells from both cortexes and hippocampus of rats exposed to RF-EMR showed a comet pattern with a clear tail representing migration of DNA having a single-strand break (Fig. 4a). Tail DNA (%), a measure of the single-strand DNA break increased significantly in both hippocampus and cortex of rats exposed to RF-EMR compared to sham animals (Fig. 4b).

3.3. Exposure to RF-EMR reduces neurogenesis in dented gyrus

We further studied the effect of RF-EMR exposure on hippocampal neurogenesis using BrdU as an endogenous marker. The BrdU-positive cells in the dented gyrus (DG) were mainly localized in the sub-

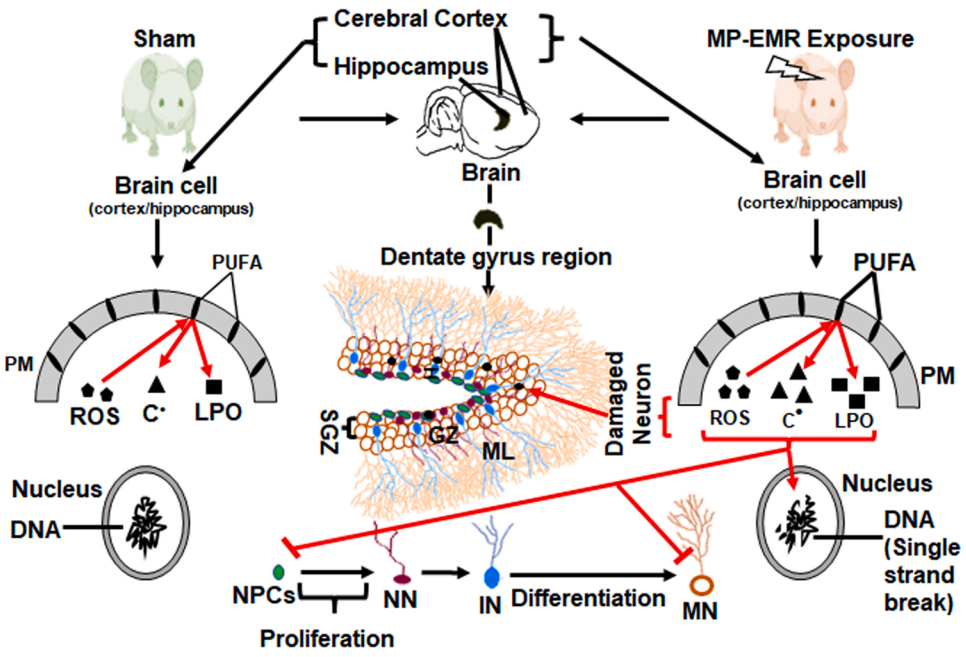


Fig. 9. Exposure to radiofrequency electromagnetic radiation (RF-EMR) seems to induce reactive oxygen species (ROS) production, which targets polyunsaturated fatty acids (PUFA) in the cerebral cortex and hippocampus cell membrane and generates carbon-centered radicals (C•) and lipid peroxides (LPO) leading to DNA damage, neuronal degeneration and impaired proliferation of hippocampal neural progenitor cells (NPCs). Important outcomes and their possible role and interrelationship at the cellular level are presented. BrdU: 5-Bromo-2′-deoxyuridine, GZ: granular zone, H: hillus, IN: immature neurons, ML: molecular layer, MN: mature neurons, NN: newborn neurons, PM: plasma membrane, RF: radiofrequency, SGZ: sub-granular zone.

granular zone. They were clustered in all animals sacrificed at either 2 or 24 h post-BrdU injection, showing diffused patterns of BrdU staining and irregularly shaped nuclei (Fig. 5a).

Quantification of BrdU-positive cells at both 24 h and 2 h time point demonstrated a significantly reduced number of BrdU-positive cells in DG of rats exposed to RF-EMR compared to shams. The number of BrdU-positive cells decreased by 1.6-fold when counted 24 h post-injection and 1.4-fold when counted 2 h post-injection, suggesting an overall reduction in neurogenesis (Fig. 5b).

Comparing the number of BrdU-positive cells at 2 h and 24 h time points in the same group provides information about the number of cells usually completing the cell cycle. DG region of sham animals had 3163 ± 443 BrdU-positive cells at 2 h and 4021 ± 456 cells at 24 h time point, amounting to a 1.3-fold increase in number. Whereas the DG region of rats exposed to RF-EMR has 2187 ± 289 BrdU-positive cells at 2 h time point and 2413 ± 413 cells at 24 h time, amounting to a 1.1-fold increase in number. These results suggest that RF-EMR exposure might also be interfering with the cell cycle progression in NPCs (Fig. 5b).

3.4. Exposure to RF-EMR causes neuronal damage in the dented gyrus

We further examined the effect of RF-EMR exposure on neuronal morphology in the cerebral cortex and subregions of the hippocampus (DG, CA3, and CA1) (Fig. 6a). Degenerating neurons were detected and quantified using Nissl staining. As visible from the photomicrograph, we observed neurons with abnormal morphology (pyknotic or karyorrhectic nuclei) predominantly in the DG region of the rat brain exposed to RF-EMR (Fig. 6b). Quantitative analysis showed a significant decrease in the percentage of neurons with normal morphology (large and abundant Nissl's bodies) in the DG of rats exposed to RF-EMR compared to shams. The degenerative changes were insignificant in the CA3 and CA1 subregions of the hippocampus and cerebral cortex (Fig. 6c).

We then investigated the effect of RF-EMR exposure on mature neurons in the cerebral cortex and hippocampal subregions using NeuN as a neuronal marker. NeuN stained photomicrographs demonstrated a noticeable neuronal loss as visible by the reduced signal intensity in the DG region of RF-EMR exposed rats (Fig. 7a). Quantitative analysis showed that the expression of NeuN protein is getting significantly decreased in the DG region of the hippocampus but not in the cerebral cortex and other subregions of the hippocampus (CA3, CA1) following the RF-EMR exposure (Fig. 7b). Based on these results, neurons in the DG region appeared to be more vulnerable to RF-EMR exposure than neurons in the other regions.

3.5. RF-EMR exposure does not activate the caspase-dependent apoptotic pathway

We further investigated whether neuronal damage observed in the DG region was due to DNA damage-induced activation of the caspase-dependent apoptotic pathway. We did not observe any significant increase in the expression of Pro caspase 3, which is a terminal marker of caspase-dependent apoptosis, in any of the brain regions upon RF-EMR exposure (Fig. 8a, b).

4. Discussion

The present study aimed to investigate the effect of short-term acute RF-EMR exposure on oxidative stress and redox-sensitive processes in the young brain. The study showed that exposure of 5-week-old male Wistar rats to 2115 MHz RF-EMR for 8 h leads to oxidative stress and DNA damage in the brain's cortex and hippocampus region along with reduced neurogenesis, and neuronal degeneration in the DG region of the hippocampus (Fig. 9). These results will augment our understanding to evaluate the effect of RF-EMR on the young adolescent brain, which is undergoing critical developmental changes and maturational processes.

We observed a significant increase in the concentration of free radicals, particularly carbon center radicals and lipid peroxides in the cortex and hippocampus regions of the rat brain upon RF-EMR exposure. However, the protein carbonyls and total antioxidant capacity have not shown a significant change in exposed rats' brain regions. Various animal models and cell line studies have reported that RF-EMR exposure causes oxidative stress (Yakymenko et al., 2016). Recent studies have proposed that RF-EMR directly activates the voltage-sensitive calcium channels in the plasma membrane resulting in excessive nitroxide signaling and peroxynitrite production which ultimately gives rise to different radical species (Pall, 2013, 2018). Few studies suggest that electromagnetic radiation generates reactive oxygen species (ROS) by targeting plasma membrane NADH oxidase (Friedman et al., 2007; Park et al., 2014). Once produced, these radical species, in turn, attack polyunsaturated fatty acids (PUFA) of the cell membrane and form

transient carbon-centered lipid radicals. These lipid radicals react with the molecular oxygen, forming lipid peroxyl radical, which ultimately decomposes into various toxic end products like aldehydes and ketones (Aruoma, 1998; Marnett, 1999). Brain tissues have a high membrane-to-cytoplasm ratio (Evans, 1993), and in the membrane, PUFA is the predominant lipid (Watson, 1993). This might be the probable reason that in this study, the effect of RF-EMR exposure is more pronounced on carbon-centered radicals and lipids than on other oxidative stress markers. Elevated radical species can also oxidize proteins and reduce the antioxidant reservoir of cells. Earlier reports have demonstrated that RF-EMR exposure causes lipid peroxidation, protein carbonylation, and diminished cellular antioxidant defense (Alkis et al., 2019, 2020). In earlier reports, repeated RF-EMR exposure was given for an extended time. However, we assessed the immediate effects of a single acute exposure to RF-EMR, which might be a reason we did not observe significant changes in the level of protein carbonyls and total antioxidant capacity.

Once produced inside the cells, different radical species, including lipid-derived radicals, may cause oxidative damage to cellular macromolecules, including nucleic acid (Marnett, 1999; Belpomme et al., 2018). In line with this fact, we also observed significant DNA damage in the cortex and hippocampus region of the rat brain exposed to RF-EMR. However, earlier studies have reported both DNA damage and no DNA damage in the brain after exposure to varying doses and durations of RF-EMR (Belyaev, 2015; Lagroye et al., 2004; Lai and Singh, 1995, 2005; Prihoda, 2019). Few animal studies also reported increased DNA damage with an increase in frequency (Alkis et al., 2019; Deshmukh et al., 2015; Megha et al., 2015) and others did not observe significant DNA damage irrespective of frequencies (Verschaeve et al., 2006). Variability in these results could be attributed to the difference in exposure and biological parameters (Belyaev, 2010). It indicates that frequency, dose and duration of exposure, and biological factors are critical for the extent of DNA damage. It has been reported that the developing brain of young adolescents is more susceptible to the RF-EMF effect (Redmayne and Johansson, 2014), and pulsed RF-EMF is more biologically active (Panagopoulos et al., 2013). The age of rats used in this study matched young adolescents and was exposed to pulse-modulated microwave frequency (2115 MHz) for 8 h. That might be a reason we observed notable DNA damage in the brain cells of exposed animals. RF-EMR-induced DNA damage might be the consequence of many carbon-centered free radicals produced under oxidative stress in the brain. The DNA damage was more pronounced in the cortex region than the hippocampus due to its proximity to the radiation source (Cardis et al., 2008) and may be due to higher absorption of RF radiation.

Radical species-mediated oxidative damage has been reported to impair neurogenesis and cell survival which in turn is associated with an increased risk of neurological disorders (Bazinet and Laye, 2014). BrdU is a thymidine analog that labels all actively dividing cells in S-phase. In the present study, we observed a reduced number of BrdU-positive cells in the DG region of rats exposed to RF-EMR compared to shams at both 2 h or 24 h post-BrdU injection time points. Two different time-points (2 h and 24 h post-BrdU injection/irradiation) were chosen, as BrdU has bioavailability for 2 h, and 24 h is the approximate cell cycle time of NPCs (Cameron and Mckay, 2001). The reduced number of BrdU-positive cells at these time points indicates that RF-EMR exposure might have led to either death of some progenitor cells or inhibited cell division or interfered with cell cycle progression in NPCs of the DG region.

We observed that in the exposure group, ~55 % of NPCs that are initially labeled (2 h time point) have completed the cell cycle (24 h time point), amounting to a 1.1-fold increase in the number of BrdU-positive cells. However, under normal conditions, for rats of this age group, about 75 % of S-phase NPCs complete the cell cycle during this time, amounting to a 1.5-fold increase in the number of BrdU-positive cells (Cameron and Mckay, 2001). The proliferating cells temporarily arrest the cell cycle in response to DNA damage to repair the lesions or lead to cellular senescence (Branzei and Foiani, 2008; De Zio et al., 2013). Hence, the RF-EMR-induced interruption of cell cycle progression might be one of the reasons among other reasons like the death of progenitor cells for a reduced number of BrdU-positive cells observed at 24 h time point and it needs further confirmation. Previous studies investigating the effect of RF-EMR exposure on adult neurogenesis, precisely in the DG region of the hippocampus, are very few. Xu et al. (2017) reported that exposure to 1.8 GHz RF-EMR for 8 h for 3 consecutive days interrupts cell division and stem cells pool in DG of newborn rats while showing no effect on the juvenile. However, Kim et al. (2015) found no effect of 848.5 MHz CDMA signal on the number of BrdU-positive cells in the DG region of young adult rats after 2 weeks of exposure. Similarly, the number of PCNA-positive cells (an early marker of neuronal proliferation) in the subventricular zone and DG of adult mice exposed to RF-EMR for 6 or 12 months (1 h daily, 5 days/week) remain unaffected (Kim et al., 2008). Our observation that younger brain and short-term acute RF-EMR exposure seem to have a more significant effect on neurogenesis corroborates earlier reports.

Histopathological observations of neurons present an idea about neuronal health and degeneration. We found markedly increased neuronal degeneration in the DG region of the hippocampus, with no significant changes in other sub-regions like CA3, CA1, and the cerebral cortex. The damaged neuronal cells have condensed chromatin, and are interspersed among normal neurons. Further, the expression of NeuN protein, which is a marker of mature neurons, also showed a significant decrease in the DG region, while there was no significant change observed in other sub-regions of the hippocampus and cortex. The results underline that the neurons in the DG region are more prone to RF-EMR-induced degeneration than in the other regions of the brain studied. It is well known that neuronal survival in the brain varies from region to region and the type of neuron (Pfisterer and Khodosevich, 2017). The immature adult-born neurons (postmitotic but not completed the maturation process) which are abundant in the DG region are more vulnerable to stress-induced death than mature ones (Leone et al., 2014; Pfisterer and Khodosevich, 2017). The high pressure to integrate into preexisting mature neuronal circuitry and high reactive oxygen species generation due to their easy excitability might be augmenting the death of adult-born neurons during the maturation (Pfisterer and Khodosevich, 2017). Whereas mature well-differentiated neurons present in non-neurogenic regions are highly resistant to death and have very efficient pro-survival mechanisms, especially against low genotoxic effects like single-strand DNA breaks for their protection for life (Kole et al., 2013; Wu et al., 2021). This might be one of the reasons that we observed significant neurodegeneration (as NeuN can also level the post-mitotic immature neurons) in the DG region upon RF-EMR exposure but not in other regions. Though to ascertain it we need to level the neuronal cell during their course of differentiation using different developmental stage-specific markers. Our results are in line with several earlier reports which have found significant neuronal degeneration in different brain regions after microwave exposure of varying frequencies, doses, and durations (Hasan et al., 2022; Kim et al., 2021; Salford et al., 2003; Sharma et al., 2019). Moreover, to understand the mechanism of neuron degeneration in the DG region we monitored the Pro-caspase3 protein, a terminal marker of the caspase-dependent apoptotic pathway. However, we didn't find any increase in its expression in any of the brain regions studied including the DG region. Many studies have reported caspase-independent neuronal death under various stress and neuropathological conditions (Vanden Berghe et al., 2015; Santiago et al., 2007; Shadfar et al., 2022). Additionally, Neuronal cells are physiologically susceptible to undergoing caspase-independent cell death as they express low labels of apaf1 protein, a component of the intrinsic apoptotic pathway, and endogenous caspases inhibitors are at a sufficient level to block the cytochrome c and apoptosis (Johnson et al., 2007; Potts et al., 2003). So, it might be possible that the neuronal degeneration we observed in the DG region is through activation of

caspase-independent cell death pathways like Ferroptosis, pyroptosis, Parthanatos, which need further investigation (Redza-Dutordoir and Averill-Bates, 2016; Shadfar et al., 2022; Tait and Green, 2008). Understanding the proapoptotic/prosurvival signaling pathways getting activated in response to RF-EMR exposure in different brain regions is our long-term interest. The findings of this study provide evidence that neurons in young brains have a high vulnerability to damage upon short-term acute exposure to RF-EMR.

5. Conclusion

In summary, this study exhibited that short-term acute exposure to RF-EMR induces oxidative stress in young adolescent rat brain regions with a marked increase in carbon-centered radicals and lipid peroxidation. Rats exposed to RF-EMR showed single-strand DNA breaks in the cortex and hippocampus, impaired hippocampal neurogenesis, and increased neuronal degeneration in the DG region. Results of the animal models have their own limitation to extrapolate for human usage but our findings suggest an adverse effect of RF-EMR in the rat brain. After careful validation, these findings may help develop appropriate interventions for reducing the impact of RF-EMR-induced adverse effects in humans.

CRediT authorship contributions statement

KVS, RKN, and PR substantially contributed to conception and design, data acquisition, analysis, and interpretation. KVS conducted the experiments. CP contributed to performing immunohistochemical experiments. JPN contributed to conducting exposure experiments and dosimetry. KVS wrote the original draft. KVS, CP, PR, and RKN edited the manuscript. RKN and PR acquired the funds and supervised the overall research work.

Ethical Approval

The experimental procedures were approved by the institutional animal ethical committee (IAEC) of Jawaharlal Nehru University, New Delhi, India (Application code # 23/2016). Experiments were performed following the committee for the purpose of control and supervision of experiments on animals (CPCSEA) guidelines and Animal Research: Reporting of In Vivo Experiments (ARRIVE) guidelines.

Declaration of Competing Interest

The authors declare that they have no known competing financial interests or personal relationships that could have appeared to influence the work reported in this paper.

Data Availability

Data will be made available on request.

Acknowledgment

This work is partly supported by the UPE II project (ID-58) and Department of Science and Technology PURSE fund of Jawaharlal Nehru University (JNU) and institute core funds from the International Center for Genetic Engineering and Biotechnology (ICGEB). KVS was supported by a fellowship from the Council of Scientific and Industrial Research (Award No. 09/263(1005)/2013-EMR-1) and the Indian Council of Medical Research (ICMR), Government of India (Award No. 849/2019); CP was supported by ICMR-RA fellowship from ICMR, Government of India. We would like to thank Ms. Subia Akram, ICGEB, and Ms. Epshita Priyadarshini, JNU for their kind help in revising the manuscript.

Appendix A. Supporting information

Supplementary data associated with this article can be found in the online version at doi:10.1016/j.neuro.2022.11.001.

References

Alkis, M.E., Bilgin, H.M., Akpolat, V., Dasdag, S., Yegin, K., Yavas, M.C., et al., 2019. Effect of 900-, 1800-, and 2100-MHz radiofrequency radiation on DNA and oxidative stress in the brain. Electromagn. Biol. Med. 38, 32–47.
Aruoma, O.I., 1998. Free radicals, oxidative stress, and antioxidants in human health and disease. J. Am. Oil Chem. Soc. 75, 199–212.
Barclay, L.R.C., Vinqvist, M.R., 1994. Membrane peroxidation: inhibiting effects of water-soluble antioxidants on phospholipids of different charge types. Free. Radic. Biol. Med. 16, 779–788.
Bas, O., Odaci, E., Mollaoglu, H., Ucok, K., Kaplan, S., 2009. Chronic prenatal exposure to the 900megahertz electromagnetic field induces pyramidal cell loss in the hippocampus of newborn rats. Toxicol. Ind. Health 25, 377–384.
Bazinet, R.P., Laye, S., 2014. Polyunsaturated fatty acids and their metabolites in brain function and disease. Nat. Rev. Neurosci. 15, 771–785.
Belpomme, D., Hardell, L., Belyaev, I., Burgio, E., Carpenter, D.O., 2018. Thermal and non-thermal health effects of low-intensity non-ionizing radiation: an international perspective. Environ. Pollut. 242, 643–658.
Belyaev, I., 2015. Electromagnetic field effects on cells and cancer risks from mobile communication. In: Rosch, P.J. (Ed.), Bioelectromagnetic and Subtle Energy Medicine, 2nd ed. CRC Press, New York, pp. 517–539.
Belyaev, I., Dean, A., Eger, H., Hubmann, G., Jandrisovits, R., Kern, M., et al., 2016. EUROPAEM EMF Guideline 2016 for the prevention, diagnosis and treatment of EMF-related health problems and illnesses. Rev. Environ. Health 31, 363–397.
Belyaev, I.Y., 2010. Dependence of non-thermal biological effects of microwaves on physical and biological variables: implications for reproducibility and safety standards. Eur. J. Oncol. Libr. 5, 187–218.
Benzie, I.F., Strain, J.J., 1996. The ferric reducing ability of plasma (FRAP) as a measure of "antioxidant power": the FRAP assay. Anal. Biochem. 239, 70–76.
Branzei, D., Foiani, M., 2008. Regulation of DNA repair throughout the cell cycle. Nat. Rev. Mol. Cell Biol. 9, 297–308.
Cameron, H.A., Mckay, R.D., 2001. Adult neurogenesis produces a large pool of new granule cells in the dentate gyrus. J. Comp. Neurol. 435, 406–417.
Cardis, E., Deltour, I., Mann, S., Moissonnier, M., Taki, M., Varsier, N., et al., 2008. Distribution of RF energy emitted by mobile phones in anatomical structures of the brain. Phys. Med. Biol. 53, 2771.
Dasdag, S., Akdag, M.Z., 2016. The link between radiofrequencies emitted from wireless technologies and oxidative stress. J. Chem. Neuroanat. 75 (Pt B), 85–93.
De Lorge, J., 1979. Operant behavior and rectal temperature of squirrel monkeys during 2.45-GHz microwave irradiation. Radio Sci. 14, 217–225.
De Zio, D., Cianfanelli, V., Cecconi, F., 2013. New insights into the link between DNA damage and apoptosis. Antioxid. Redox Signal. 19, 559–571.
Deshmukh, P.S., Nasare, N., Megha, K., Banerjee, B.D., Ahmed, R.S., Singh, D., et al., 2015. Cognitive impairment and neurogenotoxic effects in rats exposed to low-intensity microwave radiation. Int. J. Toxicol. 34, 284–290.
De-Sola Gutierrez, J., Rodríguez de Fonseca, F., Rubio, G., 2016. Cell-phone addiction: a review. Front. Psychiatry 7, 175.
Dubey, A., Forster, M.J., Lal, H., Sohal, R.S., 1996. Effect of age and caloric intake on protein oxidation in different brain regions and on behavioral functions of the mouse. Arch. Biochem. Biophys. 333, 189–197.
Durney, C.H., Iskander, M.F., Massoudi, H., Johnson, C.C., 1979. An empirical formula for broad-band SAR calculations of prolate spheroidal models of humans and animals. IEEE T. Microw. Theory 27, 758–763.
Evans, P.H., 1993. Free radicals in brain metabolism and pathology. Br. Med. Bull. 49, 577–587.
Falcioni, L., Bua, L., Tibaldi, E., Lauriola, M., De Angelis, L., Gnudi, F., et al., 2018. Report of final results regarding brain and heart tumors in Sprague-Dawley rats exposed from prenatal life until natural death to mobile phone radiofrequency field representative of a 1.8 GHz GSM base station environmental emission. Environ. Res. 165, 496–503.
Fernandez, C., de Salles, A.A., Sears, M.E., Morris, R.D., Davis, D.L., 2018. Absorption of wireless radiation in the child versus adult brain and eye from cell phone conversation or virtual reality. Environ. Res. 167, 694–699.
Foerster, M., Thielens, A., Joseph, W., Eeftens, M., Roosli, M., 2018. A prospective cohort study of adolescents' memory performance and individual brain dose of microwave radiation from wireless communication. Environ. Health Perspect. 126, 077007.
Fragopoulou, A.F., Polyzos, A., Papadopoulou, M.D., Sansone, A., Manta, A.K., Balafas, E., et al., 2018. Hippocampal lipidome and transcriptome profile alterations triggered by acute exposure of mice to GSM 1800 MHz mobile phone radiation: an exploratory study. Brain Behav. 8, e01001.
Friedman, J., Kraus, S., Hauptman, Y., Schiff, Y., Seger, R., 2007. Mechanism of short-term ERK activation by electromagnetic fields at mobile phone frequencies. Biochem. J. 405, 559–568.
Hasan, I., Rubayet, J.M., Nabiul, I.M., Rafiqul, I.M., 2022. Effect of 2400 MHz mobile phone radiation exposure on the behavior and hippocampus morphology in Swiss mouse model. Saudi J. Biol. Sci. 29 (1), 102–110.
Hyland, G.J., 2000. Physics and biology of mobile telephony. Lancet 356, 1833–1836.

IARC, 2013. Non-ionizing Radiation, Part 2: Radiofrequency Electromagnetic Fields. IARC Monographs on the Evaluation of Carcinogenic Risks to Humans/World Health Organization 102. International Agency for Research on Cancer,, p. 1.
Johnson, C.E., Huang, Y.Y., Parrish, A.B., Smith, M.I., Vaughn, A.E., Zhang, Q., et al., 2007. Differential Apaf-1 levels allow cytochrome c to induce apoptosis in brain tumors but not in normal neural tissues. Proc. Natl. Acad. Sci. USA 104, 20820–20825.
Kesari, K.K., Meena, R., Nirala, J., Kumar, J., Verma, H.N., 2014. Effect of 3G cell phone exposure with computer controlled 2-D stepper motor on non-thermal activation of the hsp27/p38MAPK stress pathway in rat brain. Cell Biochem. Biophys. 68, 347–358.
Kim, H.S., Kim, Y.J., Lee, Y.H., Lee, Y.S., Choi, H.D., Pack, J.K., et al., 2015. Effect of whole-body exposure to the 848.5 MHz code division multiple access (CDMA) electromagnetic field on adult neurogenesis in the young, healthy rat brain. Int. J. Radiat. Biol. 91, 354–359.
Kim, J.H., Lee, J.K., Kim, H.G., Kim, K.B., Kim, H.R., 2019. Possible effects of radiofrequency electromagnetic field exposure on central nerve system. Biomol. Ther. 27 (3), 265–275.
Kim, J.H., Chung, K.H., Hwang, Y.R., Park, H.R., Kim, H.J., Kim, H.G., et al., 2021. Exposure to RF-EMF alters postsynaptic structure and hinders neurite outgrowth in developing hippocampal neurons of early postnatal mice. Int. J. Mol. Sci. 22, 5340.
Kim, T.H., Huang, T.Q., Jang, J.J., Kim, M.H., Kim, H.J., Lee, J.S., et al., 2008. Local exposure of 849 MHz and 1763 MHz radiofrequency radiation to mouse heads does not induce cell death or cell proliferation in brain. Exp. Mol. Med. 40, 294–303.
Kole, A.J., Annis, R.P., Deshmukh, M., 2013. Mature neurons: equipped for survival. Cell Death Dis. 4, e689.
Lagroye, I., Anane, R., Wettring, B.A., Moros, E.G., Straube, W.L., Laregina, M., et al., 2004. Measurement of DNA damage after acute exposure to pulsed-wave 2450 MHz microwaves in rat brain cells by two alkaline comet assay methods. Int. J. Radiat. Biol. 80, 11–20.
Lai, H., Singh, N.P., 1995. Acute low-intensity microwave exposure increases DNA single-strand breaks in rat brain cells. Bioelectromagnetics 16, 207–210.
Lai, H., Singh, N.P., 2005. Interaction of microwaves and a temporally incoherent magnetic field on single and double DNA strand breaks in rat brain cells. Electromagn. Biol. Med. 24, 23–29.
Leone, L., Fusco, S., Mastrodonato, A., Piacentini, R., Barbati, S.A., Zaffina, S., et al., 2014. Epigenetic modulation of adult hippocampal neurogenesis by extremely low-frequency electromagnetic fields. Mol. Neurobiol. 49, 1472–1486.
Levin, M., 2003. Bioelectromagnetics in morphogenesis. Bioelectromagnetics 24, 295–315.
Marnett, L.J., 1999. Lipid peroxidation-DNA damage by malondialdehyde. Mutat. Res. 424, 83–95.
Megha, K., Deshmukh, P.S., Banerjee, B.D., Tripathi, A.K., Ahmed, R., Abegaonkar, M.P., 2015. Low intensity microwave radiation induced oxidative stress, inflammatory response and DNA damage in rat brain. Neurotoxicology 51, 158–165.
Miller, A.B., Sears, M., Hardell, L., Oremus, M., Soskolne, C.L., 2019. Risks to health and well-being from radio-frequency radiation emitted by cell phones and other wireless devices. Front. Public Health 7, 223.
Pall, M.L., 2013. Electromagnetic fields act via activation of voltage-gated calcium channels to produce beneficial or adverse effects. J. Cell. Mol. Med. 17 (8), 958–965.
Pall, M.L., 2016. Microwave frequency electromagnetic fields (EMFs) produce widespread neuropsychiatric effects including depression. J. Chem. Neuroanat. 75, 43–51.
Pall, M.L., 2018. Wi-Fi is an important threat to human health. Environ. Res. 164, 405–416.
Panagopoulos, D.J., Johansson, O., Carlo, G.L., 2013. Evaluation of specific absorption rate as a dosimetric quantity for electromagnetic fields bioeffects. PLoS One 8, e62663.
Park, J.E., Seo, Y.K., Yoon, H.H., Kim, C.W., Park, J.K., Jeon, S., 2014. Electromagnetic fields induce neural differentiation of human bone marrow derived mesenchymal stem cells via ROS mediated EGFR activation. Neurochem. Int. 62, 418–424.
Paxinos, G., Watson, C., 2006. The Rat Brain in Stereotaxic Coordinates: Hard Cover Edition. Elsevier.
Pfisterer, U., Khodosevich, K., 2017. Neuronal survival in the brain: neuron type-specific mechanisms. Cell Death Dis. 8 (3), e2643.
Pilla, A.A., 2012. Electromagnetic fields instantaneously modulate nitric oxide signaling in challenged biological systems. Biochem. Biophys. Res. Commun. 426, 330–333.
Potts, P.R., Singh, S., Knezek, M., Thompson, C.B., Deshmukh, M., 2003. Critical function of endogenous XIAP in regulating caspase activation during sympathetic neuronal apoptosis. J. Cell Biol. 163, 789–799.
Prihoda, T.J., 2019. Comprehensive review of quality of publications and meta-analysis of genetic damage in mammalian cells exposed to non-ionizing radiofrequency fields. Radiat. Res. 191, 20–30.
Redmayne, M., Johansson, O., 2014. Could myelin damage from radiofrequency electromagnetic field exposure help explain the functional impairment electrohypersensitivity? A review of the evidence. J. Toxicol. Environ. Health B Crit. Rev. 17, 247–258.
Redza-Dutordoir, M., Averill-Bates, D.A., 2016. Activation of apoptosis signalling pathways by reactive oxygen species. Biochim. Biophys. Acta Mol. Cell Res. 1863 (12), 2977–2992.
Rokyta, R., Stopka, P., Holecek, V., Krikava, K., Pekarkova, I., 2004. Direct measurement of free radicals in the brain cortex and the blood serum after nociceptive stimulation in rats. Neuro Endocrinol. Lett. 25, 252–258.
Sage, C., Burgio, E., 2018. Electromagnetic fields, pulsed radiofrequency radiation, and epigenetics: how wireless technologies may affect childhood development. Child Dev. 89, 129–136.
Salford, L.G., Brun, A.E., Eberhardt, J.L., Malmgren, L., Persson, B.R., 2003. Nerve cell damage in mammalian brain after exposure to microwaves from GSM mobile phones. Environ. Health Perspect. 111, 881–883.
Santiago, A.R., Cristovao, A.J., Santos, P.F., Carvalho, C.M., Ambrosio, A.F., 2007. High glucose induces caspase-independent cell death in retinal neural cells. Neurobiol. Dis. 25 (3), 464–472.
Shadfar, S., Brocardo, M., Atkin, J.D., 2022. The complex mechanisms by which neurons die following DNA damage in neurodegenerative diseases. Int. J. Mol. Sci. 23 (5), 2484.
Sharma, A., Sharma, S., Shrivastava, S., Singhal, P.K., Shukla, S., 2019. Mobile phone induced cognitive and neurochemical consequences. J. Chem. Neuroanat. 102, 101684.
Singh, K.V., Gautam, R., Meena, R., Nirala, J.P., Jha, S.K., Rajamani, P., 2020. Effect of mobile phone radiation on oxidative stress, inflammatory response, and contextual fear memory in Wistar rat. Environ. Sci. Pollut. Res. 27 (16), 19340–19351.
Singh, K.V., Arya, R., Nirala, J.P., Sahu, D., Nanda, R.K., Rajamani, P., 2022. Effects of mobile phone electromagnetic radiation on rat hippocampus proteome. Environ. Toxicol. 37 (4), 836–847.
Stein, Y., Udasin, I.G., 2020. Electromagnetic hypersensitivity (EHS, microwave syndrome) - Review of mechanisms. Environ. Res. 186, 109445.
Sudan, M., Olsen, J., Arah, O.A., Obel, C., Kheifets, L., 2016. Prospective cohort analysis of cellphone uses and emotional and behavioral difficulties in children. J. Epidemiol. Community Health 70, 1207–1213.
Tait, S., Green, D., 2008. Caspase-independent cell death: leaving the set without the final cut. Oncogene 27, 6452–6461.
Uchiyama, M., Mihara, M., 1978. Determination of malonaldehyde precursor in tissues by thiobarbituric acid test. Anal. Biochem. 86, 271–278.
Vanden Berghe, T., Kaiser, W.J., Bertrand, M.J., Vandenabeele, P., 2015. Molecular crosstalk between apoptosis, necroptosis, and survival signaling. Mol. Cell. Oncol. 2 (4), e975093.
Verschaeve, L., Heikkinen, P., Verheyen, G., Van Gorp, U., Boonen, F., Vander Plaetse, F., et al., 2006. Investigation of co-genotoxic effects of radiofrequency electromagnetic fields in vivo. Radiat. Res. 165, 598–607.
Wainwright, P., 2000. Thermal effects of radiation from cellular telephones. Phys. Med. Biol. 45, 2363.
Watson, B.D., 1993. Evaluation of the concomitance of lipid peroxidation in experimental models of cerebral ischemia and stroke. Prog. Brain Res. 96, 69–95.
Wu, W., Hill, S.E., Nathan, W.J., Paiano, J., Callen, E., Wang, D., et al., 2021. Neuronal enhancers are hotspots for DNA single-strand break repair. Nature 593, 440–444.
Xu, F., Bai, Q., Zhou, K., Ma, L., Duan, J., Zhuang, F., et al., 2017. Age-dependent acute interference with stem and progenitor cell proliferation in the hippocampus after exposure to 1800 MHz electromagnetic radiation. Electromagn. Biol. Med. 36, 158–166.
Yakymenko, I., Tsybulin, O., Sidorik, E., Henshel, D., Kyrylenko, O., Kyrylenko, S., 2016. Oxidative mechanisms of biological activity of low-intensity radiofrequency radiation. Electromagn. Biol. Med. 35, 186–202.
Yang, H., Zhang, Y., Wu, X., Gan, P., Luo, X., Zhong, S., Zuo, W., 2022. Effects of acute exposure to 3500 MHz (5G) radiofrequency electromagnetic radiation on anxiety-like behavior and the auditory cortex in guinea pigs. Bioelectromagnetics 43, 106–118.
Youssef, M., Atsak, P., Cardenas, J., Kosmidis, S., Leonardo, E.D., Dranovsky, A., 2019. Early life stress delays hippocampal development and diminishes the adult stem cell pool in mice. Sci. Rep. 9, 4120.
Yuan, K., Qin, W., Wang, G., Zeng, F., Zhao, L., Yang, X., et al., 2011. Microstructure abnormalities in adolescents with internet addiction disorder. PLoS One 6, e20708.

Web References

Common Sense Media, 2019. The common-sense census: Media use by tweens and teens. ⟨https://www.commonsensemedia.org/research/the-common-sense-census-media-use-by-tweens-and-teens-2019⟩ (accessed 30th January 2022).
Anon. ⟨https://bioinitiative.org⟩. Accessed March 24, 2022.
Anon. ⟨https://www.bfs.de/SiteGlobals/Forms/Suche/BfS/EN/SARsuche_Formular.html?nn= 6008110&csstring_SARAdditional=aktuell⟩. Accessed April 28, 2022.
Anon. ⟨https://www.statista.com/topics/1147/mobile-communications/#dossierKeyfigures⟩. Accessed April 28, 2022.